Euro. Jnl of Applied Mathematics: page 1 of 20 © The Author(s), 2021. Published by Cambridge University Press. 1
doi:10.1017/S0956792520000431

Spikes and localised patterns for a novel Schnakenberg model in the semi-strong interaction regime

FAHAD AL SAADI[1,2], ALAN CHAMPNEYS[1], CHUNYI GAI[3] and THEODORE KOLOKOLNIKOV[3]

[1]*Department of Engineering Mathematics, University of Bristol, Bristol BS8 1UB, UK*
emails: a.r.champneys@bristol.ac.uk; fa17741@bristol.ac.uk
[2]*Department of Systems Engineering, Military Technological College, Muscat, Oman*
[3]*Department of Mathematics and Statistics, Dalhousie University, Halifax, Nova Scotia B3H 4R2, Canada*
emails: Chunyi.Gai@dal.ca; tkolokol@gmail.com

(*Received 19 May 2020*; *revised 25 November 2020*; *accepted 6 December 2020*)

An analysis is undertaken of the formation and stability of localised patterns in a 1D Schanckenberg model, with source terms in both the activator and inhibitor fields. The aim is to illustrate the connection between semi-strong asymptotic analysis and the theory of localised pattern formation within a pinning region created by a subcritical Turing bifurcation. A two-parameter bifurcation diagram of homogeneous, periodic and localised patterns is obtained numerically. A natural asymptotic scaling for semi-strong interaction theory is found where an activator source term $a = \mathcal{O}(\varepsilon)$ and the inhibitor source $b = \mathcal{O}(\varepsilon^2)$, with ε^2 being the diffusion ratio. The theory predicts a fold of spike solutions leading to onset of localised patterns upon increase of b from zero. Non-local eigenvalue arguments show that both branches emanating from the fold are unstable, with the higher intensity branch becoming stable through a Hopf bifurcation as b increases beyond the $\mathcal{O}(\varepsilon)$ regime. All analytical results are found to agree with numerics. In particular, the asymptotic expression for the fold is found to be accurate beyond its region of validity, and its extension into the pinning region is found to form the low b boundary of the so-called homoclinic snaking region. Further numerical results point to both sub and supercritical Hopf bifurcation and novel spikeinsertion dynamics.

Key words: reaction-diffusion systems, pattern formation, spikes, snaking

2020 Mathematics Subject Classification: Primary: 35B32; Secondary: 35K57, 92C15, 34E13

1 Introduction

Since the pioneering work of Alan Turing [28], there has been significant interest in the theory of pattern formation in reaction diffusion systems. Various canonical models of activator inhibitor type have been proposed, such as those due to Gierer & Meinhardt [9] and Schnakenberg [24], that have been found to replicate spatio-temporal behaviour across the natural world. Indeed, the Turing theory of pattern formation is now a core topic within mathematical biology; see, e.g. the books by Murray and Meron [21, 18]. Turing instabilities describe the onset of small-amplitude periodic patterns. More recent theories using either formal semi-strong asymptotic expansions

(see, e.g. [19, 20, 11, 30, 12, 17] and references therein) or geometric singular perturbation theory (see, e.g. [7, 8] and references therein) have led to theories showing existence and dynamics of more complex, large amplitude patterns.

In recent years, there has been a parallel interest in the formation and dynamics of spatially localised patterns in systems described by higher order scalar equations such as generalisations of the Swift-Hohenberg model [27]. The theory relies on the formation of localised states of arbitrarily wide spatial extent within the Pomeau [22] pinning region due to the phenomenon known as homoclinic snaking [33, 5, 2]. See, for example, the reviews by Knobloch [13, 14].

The aim of this paper is to show how these two theoretical paradigms fit together by studying a variant of Schnakenberg model in one spatial dimension with source terms in both activator and inhibitor fields. In particular, we aim to show how the semi-strong asymptotic analysis applied in the limit of an infinite domain can show the onset of large amplitude exponentially localised patterns through a fold bifurcation. Here, semi-strong implies a scaling where the activator field is much more highly localised than the inhibitor. When this fold is followed numerically into a different pattern regime, we find that it forms the extremity of the homoclinic snaking region. Moreover, the semi-strong limit allows for analysis of the stability of the localised patterns. By introducing a small parameter τ associated with the timescale of the inhibitor field, we are able to appeal to the theory of non-local eigenvalue problems. This theory can then be extended to argue the existence of a temporal Hopf bifurcation as one passes from the snaking regime to the semi-strong limit.

The rest of this paper is outlined as follows. Section 2 presents the system under investigation, the stability of its homogeneous state and a numerical overview of regions of existence of periodic and localised patterns. Section 3 then considers the adaptation of semi-strong asymptotic theory to show existence of localised patterns on an infinite domain. Section 4 considers stability analysis of the localised patterns using non-local eigenvalue problem theory. In both Sections 3 and 4, the theory is shown to agree well with numerics. Finally, Section 5 draws conclusions and points to the wider implications of the work.

2 The Schnakenberg model and its underlying dynamics

The model in question was first proposed in [24] and has many applications in biology; see, e.g. [3, 25] and references therein. The equations describe an autocatalytic reaction between two chemical products X, Y and two sources A and B as follows:

$$U <=> A, \quad B \to V, \quad 2U + V \to 3U.$$

The reaction takes place in a closed domain, such that the activator U and inhibitor V are free to diffuse in one spatial dimension, across a domain of size $2l$, and that the sources A and B are abundant everywhere and do not diffuse. Applying the law of mass action, then after non-dimensionalisation, one can obtain the following system of reaction diffusion equations:

$$\frac{\partial u}{\partial t} = a - u + u^2 v + \varepsilon^2 \frac{\partial^2 u}{\partial x^2}, \quad -l < x < l, \quad t > 0 \tag{2.1a}$$

$$\frac{\partial v}{\partial t} = b - u^2 v + \frac{\partial^2 v}{\partial x^2}, \quad -l < x < l, \quad t > 0 \tag{2.1b}$$

$$u_x(\pm l, t) = v_x(\pm l, t) = 0. \tag{2.1c}$$

Here u and v represent the activator and the inhibitor concentration, respectively, and the parameters $a, b > 0$ are the respective constant concentrations of A and B. The dimensionless parameter $\varepsilon > 0$ measures the ratio of the diffusion rate of the activator to that of the inhibitor. In what follows we shall be interested in the case that $0 < \varepsilon \ll 1$ and in the limit of an infinitely long domain $l \to \infty$.

Upon setting the diffusion terms in (2.1) to zero, a straightforward calculation shows there is a unique homogeneous equilibrium:

$$(u_s, v_s) = \left(a + b, \frac{b}{(a+b)^2}\right). \tag{2.2}$$

Standard linear stability analysis around (2.2) gives conditions for a pattern formation, or Turing instability with wavenumber $k \in \mathbb{R}$. Specifically, substitution of the ansatz

$$(u, v) = (u_s, v_s) + (\bar{U}, \bar{V})e^{ikx+\lambda t}, \qquad \text{with} \quad ||\bar{U}, \bar{V}|| \ll 1.$$

into (2.1), after, excluding nonlinear terms, gives a condition for the loss of stability under variation of a parameter:

$$\Re(\lambda(k_c)) = 0, \quad \text{and} \quad \Re(\partial_k \lambda(k_c)) = 0.$$

Here, λ is the temporal eigenvalue of (2.2) and k_c is the critical value of the wavenumber. Proceeding in the usual way, we obtain the condition for Turing instability and the critical wave number as

$$b - (a+b)^3 \varepsilon^2 - a = 2\ (a+b)^2 \varepsilon, \tag{2.3}$$

$$k_c^2 = \frac{-(a+b)^3 \varepsilon^2 - a + b}{2\varepsilon^2 (a+b)}.$$

As argued, for example, in [4], the above conditions for a temporal Turing bifurcation can be interpreted as a so-called Hamiltonian–Hopf bifurcation in terms of spatial dynamics (that is when the time-independent problem is posed on the infinite domain and the spatial variable x is considered to be time-like, see, e.g. [10]). Another linear transition we shall be interested in is when the far field of the purely spatial problem posed around the homogeneous equilibrium switches from having monotone to oscillatory decay. Such a Belyakov–Devaney (BD) transition occurs whenever there is a pair of double real eigenvalues of the spatial dynamics problem linearised about the homogeneous equilibrium. This gives the condition

$$b - (a+b)^3 \varepsilon^2 - a = -2\ (a+b)^2 \varepsilon. \tag{2.4}$$

The curve (2.3) is plotted in Figure 1(a) in the (a, b)-plane for fixed ε (solid red line). Using weakly nonlinear analysis (details not presented) we find that for sufficiently large a, stable periodic patterns bifurcate supercritically from the Turing bifurcation as b increases (into the yellow shaded region in the figure). For smaller a, the bifurcation is subcritical and a fold in the periodic structures occurs for lower b values, creating a Pomeau pinning region (shaded green in the figure) in which localised structures are observed. The large a limit of the localised structures region is formed by the codimension-two point where the Turing bifurcation changes from being sub- to supercritical (indicated by the pink circle in the figure).

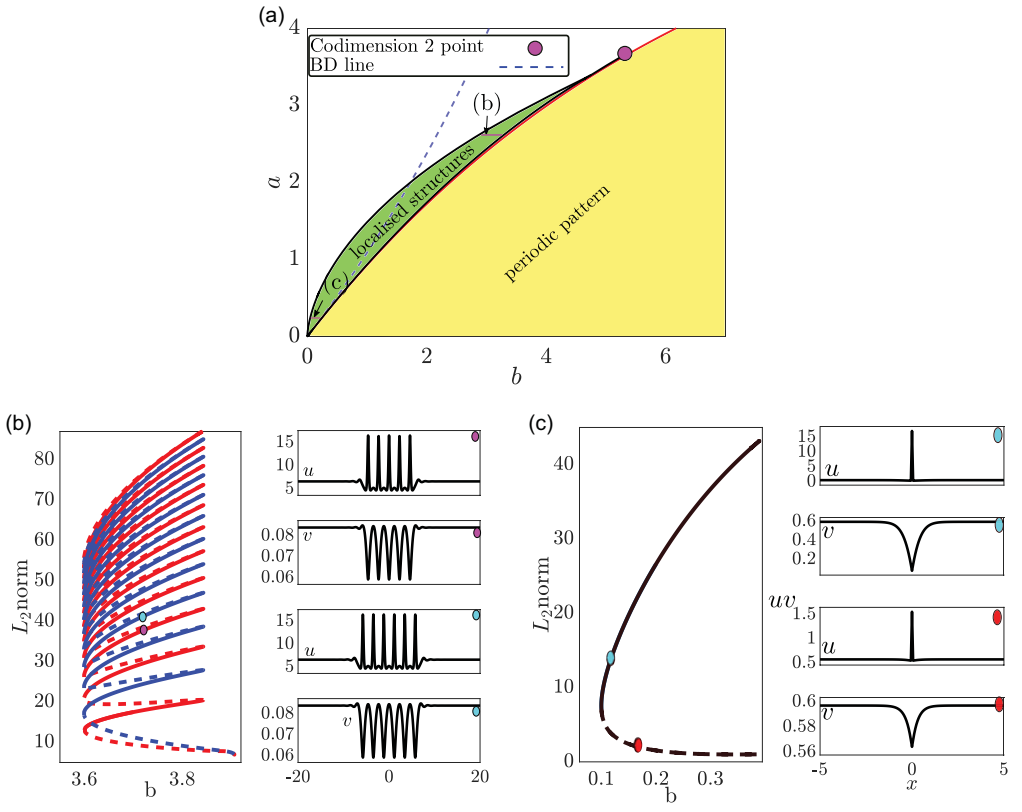

FIGURE 1. Color version online. (a) The (b, a) bifurcation diagram for fixed $\varepsilon = 0.01$ and $l = 100$. The red curve represents a Turing bifurcation and black lines represent the (outer) folds of a bifurcation diagram of localised solutions. (b) One-parameter numerical bifurcation diagram showing snaking of multi-pulsed solutions for $a = 3$ as b varies. A continuous (or dashed) line indicates where spectral computation indicates that the solution is stable (unstable). A red (blue) colour indicates that the number of peaks in the solution is odd (even). Insets show u and v solution profiles at the two indicated points in the bifurcation diagram. (c) One-parameter numerical bifurcation diagram as b varies for $a = 0.3785$ where a fold bifurcation connects spike solutions that are computed to be stable (unstable) as indicated by a continuous (dashed) line. Insets show the u and v solution profiles at the indicated points.

Figure 1 also contains numerical results obtained using AUTO [6] on the bifurcation structure of localised solutions within the green shaded region. Details of the analytical and numerical methods used will be presented elsewhere [1], which will also point to the ubiquity of this overall shape of bifurcation diagram to other reaction-diffusion systems.

The BD curve defined by (2.4) is also depicted in Figure 1(a); note how it divides the localised structure region into two parts. The region to the right of the BD line is where spatial eigenvalues are complex and localised solutions have oscillatory tails, whereas to the left line, the spatial eigenvalues are purely real and solutions have monotonic tails. Recently [29], in a class of reaction diffusion equations which includes (2.1), it is argued that a single-spike localised pattern crossing a BD from right to left in the sense of Figure 1(a) should result in the destruction of all but a finite number of localised pattern solutions. Effectively, the infinitely many additional stable multi-pulse solutions to the right become delocalised in the limit of the BD line, via the

distance between their large peaks tending to infinity. Figure 1(b) and (c) show one-parameter bifurcation diagrams of localised structures obtained numerically, which appear to confirm this prediction. The figures also indicate which among the various solutions are found numerically to be stable.

In particular note that the localised solutions for small a and b shown in the inset to Figure 1(c) consists of a highly localised spike in u, but is more spread out in the inhibitor field v. This observation is suggestive that there may be a semi-strong asymptotic analysis that can predict the bifurcation diagram observed for these two spike solutions. Note that the v field appears exponentially localised, which would suggest a different approach to the finite-domain assumption typically used in previous works, e.g. [15, 30] in which the v field is approximately two reflected quadratic functions.

A related fold point has been studied for the Gray–Scott model (where $a = 0$, and which also includes a decay term in the v equation). See, for example, [7, 19, 20, 16] where such fold point and related stability properties were analysed on either infinite or bounded domains.

3 Semi-strong asymptotic construction of spike solutions

Consider the steady-state system version of (2.1):

$$a - u + u^2 v + \varepsilon^2 \frac{\partial^2 u}{\partial x^2} = 0, \quad x \in (-l, l), \tag{3.1a}$$

$$b - u^2 v + \frac{\partial^2 v}{\partial x^2} = 0, \quad x \in (-l, l), \tag{3.1b}$$

subject to Neumman boundary conditions. We are interested in the limit that $l \to \infty$, in which case we shall seek a solution of (3.1) that is a homoclinic orbit in space to the homogeneous equilibrium

$$u \to a + b, \qquad v \to \frac{b}{(a+b)^2}, \quad \text{as } x \to \pm\infty.$$

The semi-strong interaction method [30] is a form of matched asymptotic expansion which applies to the current problem when both parameters a and b are small. In particular, we find a natural distinguished limit by setting

$$a = \varepsilon\, \alpha, \qquad b = \varepsilon^2\, \beta, \qquad \text{where } \alpha \text{ and } \beta \text{ are } O(1), \tag{3.2}$$

to obtain

$$0 = \varepsilon^2 \frac{\partial^2 u}{\partial x^2} + u^2 v - u + \varepsilon\alpha, \tag{3.3a}$$

$$0 = \frac{\partial^2 v}{\partial x^2} + \varepsilon^2 \beta - u^2 v. \tag{3.3b}$$

We then seek solutions expanded in powers of ε

$$u(x) = u_0 + \varepsilon u_1 + O(\varepsilon^2), \qquad v(x) = v_0 + \varepsilon v_1 + O(\varepsilon^2),$$

in the inner and outer asymptotic regimes, separately.

3.1 Inner solution

Without loss of generality, assume that the centre of the spike solution is at $x = 0$, and introduce a new spatial coordinate given via

$$x = \varepsilon y. \tag{3.4}$$

Collecting leading order terms of system (3.3), we obtain

$$u_{0yy} - u_0 + u_0^2 v_0 = 0, \tag{3.5a}$$

$$v_{0yy} = 0. \tag{3.5b}$$

Solving system (3.5), we find that v_0 is a constant to be determined

$$v_0 \equiv \kappa. \tag{3.6}$$

Then, from the u equation we need to find a solution

$$u_0 = (1/\kappa) w(y), \tag{3.7}$$

where $w(y)$ satisfies

$$w'' - w + w^2 = 0, \quad -\infty < y < \infty, \tag{3.8a}$$

$$w \to 0 \quad as \quad y \to \pm\infty; \quad w'(0) = 0, \quad w(0) > 0. \tag{3.8b}$$

The unique solution to (3.8) is

$$w(y) = \frac{3}{2}\mathrm{sech}^2\left(\frac{y}{2}\right). \tag{3.9}$$

3.2 Outer solution

We introduce a new scaling within an outer region, given by

$$x = \frac{z}{\varepsilon}, \quad u = \varepsilon \hat{u}(z), \quad v = \hat{v}(z).$$

Collecting terms in (3.3) that have the same order of ε to leading order we find

$$\hat{u}_0(z) = \alpha, \qquad \text{and} \qquad \hat{v}_{0zz} - \hat{u}_0^2 \hat{v}_0 + \beta = 0.$$

However, it is useful to include the $O(\varepsilon)$-correction to the u solution, so that we can match the asymptotic boundary conditions exactly in the limit $l \to \infty$. That is,

$$\hat{u}(z) = \alpha + \varepsilon\beta, \tag{3.10}$$

in which case, we find that the leading order solution for v needs to satisfy

$$v \sim \frac{\beta}{(\alpha + \varepsilon\beta)^2} \text{ when } |z| \gg 1.$$

In the outer region, we solve separately on the intervals $z \in [-\varepsilon l, 0]$ and $z \in [0, \varepsilon l]$. Solving separately on these domains, we get

$$\hat{u}(z) = \alpha + \varepsilon\beta,$$

and

$$\hat{v}(z) = \frac{\left(\kappa(\alpha+\varepsilon\beta)^2 - \beta\right)}{(\alpha+\varepsilon\beta)^2\cosh(\varepsilon l(\alpha+\varepsilon\beta))}\cosh((\alpha+\varepsilon\beta)\,(|z|-\varepsilon l)) + \frac{\beta}{(\alpha+\varepsilon\beta)^2}. \tag{3.11}$$

In the limit $l \to \infty$, this function can be written as

$$\hat{v}(z) = \left(\kappa - \frac{\beta}{(\varepsilon\beta+\alpha)^2}\right)\exp\left[-(\varepsilon\beta+\alpha)|z|\right] + \frac{\beta}{(\varepsilon\beta+\alpha)^2}.$$

3.3 Matching

In order to match inner and outer solutions, we have freedom to choose a value of the free variable κ. A typical approach would be to match derivatives of the inner and outer solutions at $x = 0$. But the outer solution is not differentiable there. So, following Ward et al. [30] we look to match the solutions in a weak sense. The novelty here though is to use a matching method that does not rely on l being finite.

Adding the inner and outer solutions from the previous sections, we obtain

$$u(x) = \frac{3}{2\kappa}\mathrm{sech}^2\left(\frac{y}{2}\right) + \varepsilon\hat{u}\left(\frac{z}{\varepsilon}\right), \quad v(x) = \hat{v}\left(\frac{z}{\varepsilon}\right),$$

which we then substitute into a weak form of the v equation:

$$\int_{\text{inner}} [\,\varepsilon^2\beta - u^2 v + v_{xx}\,]dx = 0 \tag{3.12}$$

in the limit $\varepsilon \to 0$. Here, the domain of integration corresponds to an extended interval around the inner asymptotic region that includes a matching zone: $\int_{\text{inner}} = \int_{-\delta}^{\delta}$ where δ is an arbitrary number, assumed to have the asymptotic order $\varepsilon \ll \delta \ll 1$.

It would seem that condition (3.12) for the matching of the inner and outer solutions (which contrasts with that in [30] where integration is taken over the entire outer domain) can be seen as somewhat akin to the vanishing of a Melnikov integral, as used in geometric singular perturbation theory, e.g. [8]. A detailed comparison between the different asymptotic theories is beyond the scope of this paper.

Consider the three terms in the integrand of (3.12) separately. The first term integrates to zero because $\varepsilon^2\beta$ is vanishingly small in the limit $\varepsilon \to 0$. The second term can be approximated as

$$\int_{-\infty}^{\infty} \varepsilon\kappa u_0^2(y)dy = \int_{-\infty}^{\infty} \frac{\varepsilon}{\kappa}\mathrm{sech}^4\left(\frac{y}{2}\right)dy = \frac{6\varepsilon}{\kappa}. \tag{3.13}$$

Finally, the third term can be approximated as

$$\int_{0^-}^{0^+} \hat{v}_{zz}dz = [\hat{v}_z]_{0^+} - [\hat{v}_z]_{0^-} = -2\left(\kappa - \frac{\beta}{(\alpha+\varepsilon\beta)^2}\right)\varepsilon\,(\alpha+\varepsilon\beta)\tanh(\varepsilon\alpha l). \tag{3.14}$$

Substitution of (3.13) and (3.14) into (3.12) yields the following quadratic equation for κ

$$\left(-2\,(\alpha+\varepsilon\beta)\,\kappa^2 + \frac{2\beta\kappa}{(\alpha+\varepsilon\beta)}\right)\varepsilon\tanh(\varepsilon\alpha l) - 6\varepsilon = 0. \tag{3.15}$$

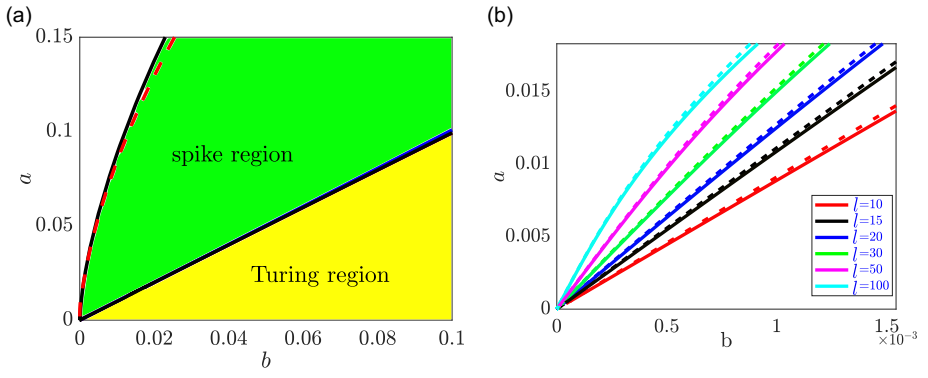

FIGURE 2. Colour version online. A zoom of the spike region of Figure 1. (a) The dashed red line indicates the analytical upper expression (3.18) in the limit $l \to \infty$, which can be compared to the the solid black fold line computed numerically. (b) The corresponding fold curves for different finite values of l; with dashed (solid) lines representing analytic (numerical) approximations.

Note that when $l \to \infty$, $\tanh(\varepsilon\alpha l) \sim 1$, which yields

$$-2(\alpha + \varepsilon\beta)\,\kappa^2 + \frac{2\beta\kappa}{(\alpha + \varepsilon\beta)} - 6 = 0. \tag{3.16}$$

On the other hand, the domain l must be much larger than the width of the spike in order for the asymptotics to be consistent. This means that we must assume $l \gg O(\varepsilon)$.

Solving (3.16), we obtain two values for κ, which correspond to a small and a large value. Specifically,

$$\kappa_1 = \frac{\beta - \sqrt{-12\ (\varepsilon\beta + \alpha)^3 + \beta^2}}{2\,(\varepsilon\beta + \alpha)^2}, \tag{3.17a}$$

$$\kappa_2 = \frac{\beta + \sqrt{-12\ (\varepsilon\beta + \alpha)^3 + \beta^2}}{2\,(\varepsilon\beta + \alpha)^2}. \tag{3.17b}$$

We shall refer to κ_1 as corresponding to an 'upper branch' of the spike solution, and κ_2 to a 'lower branch'. Finally, we can find a fold bifurcation of spikes by setting the discriminant of (3.15) to zero, which gives a curve in the (a, b) plane given by

$$\beta^2 \tanh(\varepsilon\alpha l) - 12\,(\alpha + \varepsilon\beta)^3 = b^2 \tanh(al) - 12\,\varepsilon\,(a + b)^3 = 0. \tag{3.18}$$

The two spike solutions exist for a values less that this curve, and b values above it.

3.4 Comparison with numerics

Figure 2(a) plots a zoom of the left-hand corner of Figure 1(a), comparing the computed left and fold with the formula (3.18) in the limit $l \to \infty$ as a red dashed line. It is clear that the two lines are in good agreement in the limit of small a and b where the asymptotic analysis applies. Figure 2(b) shows (3.18) for different values of l (dashed lines) which is again shown to have good agreement with the corresponding numerical results from AUTO.

Figures 3 and 4 show a comparison between the approximate solutions obtained via asymptotic analysis and the corresponding numerical solution obtained using AUTO. It is clear from

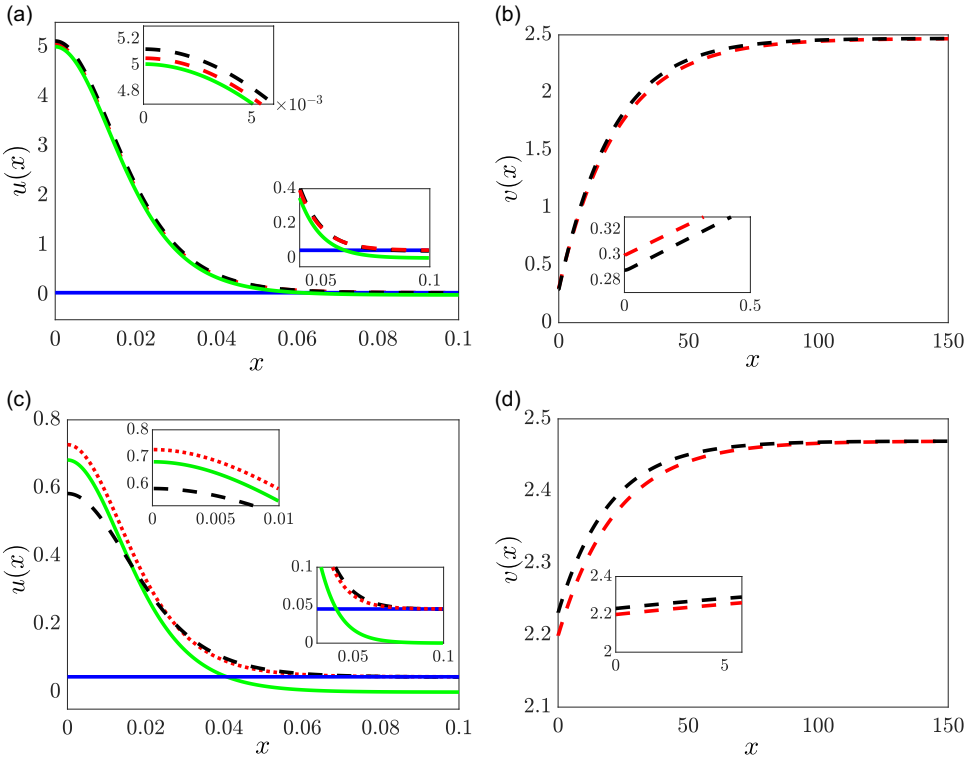

FIGURE 3. Color version online. Comparison between the semi-strong asymptotic solution and the numerical solution for $a = 0.04$, $b = 0.005$ and $\varepsilon = 0.01$ in the limit $l \to \infty$ (computations performed with $l = 1000$). (a) Solution profile $u(x)$ for $x > 0$ on the upper branch; green and blue continuous lines indicate the inner and the outer solution, respectively. The red dashed lines represent the sum of the inner and outer solutions, and the black dashed line is the numerical solution. (b) Solution profile for $v(x)$ for $x > 0$ on the upper branch with red and black dashed lines indicating the analytical and numerical solutions, respectively. (c)–(d) Solutions for the lower branch plot identically to panels (a)–(b), respectively.

the figures that there is good agreement for both the upper/stable and lower/unstable branch of solutions, both on a finite domain and an infinite domain. Note how the agreement gets better as $l \to \infty$. Also note how the v component transforms from being exponentially localised to being more quadratic-shaped as l is decreased from $+\infty$.

4 Stability analysis

In this section we consider linear stability of a spike. Our analysis is closely related to [31, 32] and uses the results on the related Non-local Eigenvalue Problem (NLEP) therein.

We start by considering a more general case where the timescales of the two fields are different. Specifically, let us assume that a time scaling parameter τ multiplies v_t, so that system (2.1) becomes

$$u_t = \varepsilon^2 u_{xx} - u + u^2 v + \varepsilon\alpha, \tag{4.1a}$$

$$\tau v_t = v_{xx} - u^2 v + \varepsilon^2 \beta\,. \tag{4.1b}$$

It will be convenient to consider τ at first to be small, and then continue up to the case $\tau = 1$, which leads to (2.1).

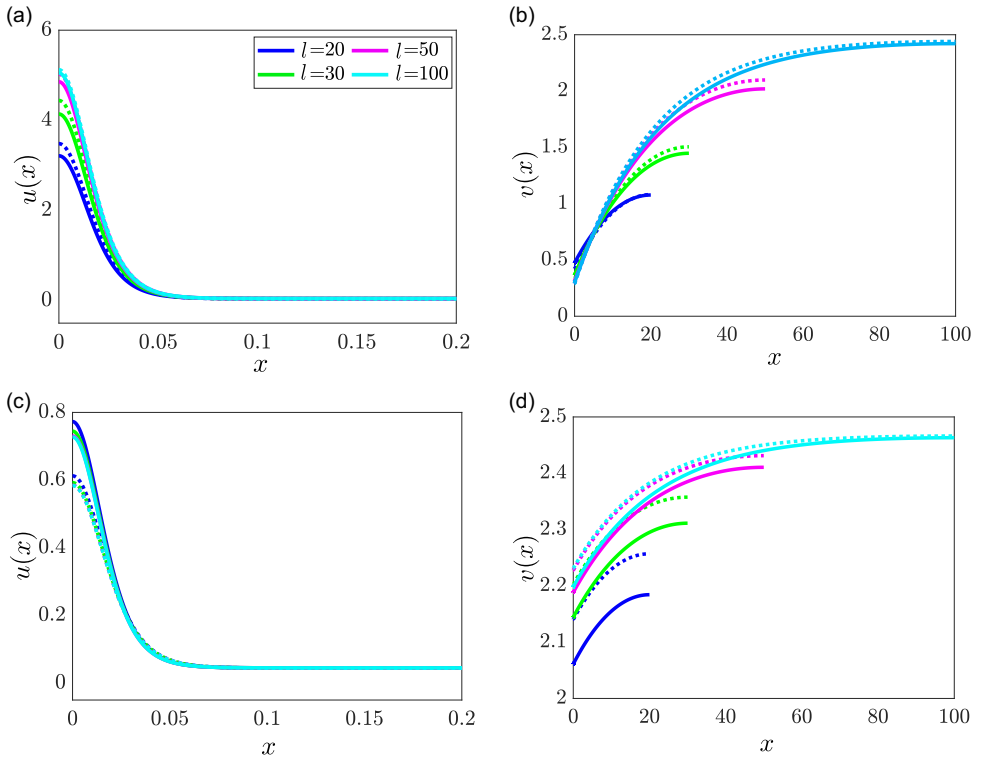

FIGURE 4. Colour version online. Similar to Figure 3 but on a finite domain. (a) and (b) Analytical approximations to solution profiles for $u(x)$ and $v(x)$, respectively, for the upper branch (solid lines) and their numerically obtained counterparts (dashed lines). (c)–(d) Solutions for the lower branch plot identically to panels (a)–(b), respectively.

4.1 A non-local eigenvalue problem

We first linearise around steady state by taking

$$u(x,t) = u_0(x) + \phi(x)\exp(\lambda t),$$
$$v(x,t) = v_0(x) + \psi(x)\exp(\lambda t),$$

where we assume $|\phi|, |\psi| \ll 1$. Then we obtain the linearised problem

$$\lambda\phi = \varepsilon^2\phi_{xx} + (2u_0v_0 - 1)\phi + u_0^2\psi,$$
$$\tau\lambda\psi = \psi_{xx} - 2u_0v_0\phi - u_0^2\psi\,.$$

In the inner region, we let $y = \frac{x}{\varepsilon}$, then to leading order we obtain $\psi_{yy} = 0$ so that $\psi \sim \psi_0$ is a constant which needs to be determined. The equation for ϕ then becomes

$$\lambda\phi = \phi_{yy} + 2w\phi - \phi + \frac{w^2}{\kappa^2}\psi_0. \tag{4.2}$$

In the outer region, we approximate

$$\psi_{xx} - \tau\lambda\psi - \varepsilon^2\alpha^2\psi = c\delta(x;0), \tag{4.3}$$

where

$$c = 2\int_{0-}^{0+} u_0 v_0 \phi dx + \int_{0-}^{0+} u_0^2 \psi dx$$
$$\sim 2\varepsilon \int_{-\infty}^{\infty} \phi w dy + \frac{6\varepsilon}{\kappa^2}\psi_0\,, \quad \text{as } \varepsilon \to 0$$

in which we have used the fact that $\int_{-\infty}^{\infty} w^2 dy = 6$. The solution to (4.3) can be written as

$$\psi = cG(x;\mu),\ \mu = \sqrt{\tau\lambda + \varepsilon^2\alpha^2}$$

where $G(x;\mu)$ is the Green's function which satisfies

$$\begin{cases} G_{xx} - \mu^2 G = \delta(x;0), \\ \quad G_x(\pm l) = 0\,, \end{cases}$$

and

$$G(x;\mu) = -\frac{1}{2\mu\sinh(\mu l)}\cosh(\mu(|x| - l)).$$

Therefore the solution to (4.3) is

$$\psi(x) = -\frac{c}{2\sqrt{\tau\lambda + \varepsilon^2\alpha^2}\sinh(\sqrt{\tau\lambda + \varepsilon^2\alpha^2}l)}\cosh(\sqrt{\tau\lambda + \varepsilon^2\alpha^2}(|x| - l)),$$

and we solve ψ_0 by letting

$$\psi_0 = \psi(0) = -\frac{\varepsilon\int \phi w dy + \frac{3\varepsilon}{\kappa^2}\psi_0}{\sqrt{\tau\lambda + \varepsilon^2\alpha^2}\tanh(\sqrt{\tau\lambda + \varepsilon^2\alpha^2}l)}$$

so that

$$\psi_0 = -\frac{\varepsilon\int \phi w dy}{\frac{3\varepsilon}{\kappa^2} + \sqrt{\tau\lambda + \varepsilon^2\alpha^2}\tanh(\sqrt{\tau\lambda + \varepsilon^2\alpha^2}l)}. \tag{4.4}$$

Substituting (4.4) into (4.2) yields the following non-local eigenvalue problem (NLEP)

$$\lambda\phi = L_0\phi - w^2\frac{\int \phi w dy}{A}, \tag{4.5}$$

where $L_0\phi = \phi_{yy} - \phi + 2w\phi$ and

$$A = 3 + \sqrt{\frac{\tau\lambda}{\varepsilon^2} + \alpha^2}\tanh(\sqrt{\tau\lambda + \varepsilon^2\alpha^2}l)\kappa^2. \tag{4.6}$$

To analyse stability, we consider the following two cases $\tau = 0$ and $\tau \neq 0$.

4.2 The case $\tau = 0$

When taking $\tau = 0$, A in (4.6) simplifies to

$$A = 3 + \alpha\tanh(\varepsilon\alpha l)\kappa^2, \tag{4.7}$$

then equation (4.5) reduces to a well-known NLEP which is first studied in [32], in particular, we have the following basic result:

Theorem 1 *(See [32]) Consider the problem (4.5), we have* $Re(\lambda) < 0$ *if* $A < 6$, $Re(\lambda) > 0$ *if* $A > 6$, *and* $\lambda = 0$ *with* $\phi = w$ *if* $A = 6$.

To determine the stability of two branches corresponding to the values κ_1 and κ_2 shown in (3.17), we substitute $\kappa_{1,2}$ into (4.7) to obtain

$$A(\kappa_{1,2}) = \frac{\beta^2 \tanh(\varepsilon\alpha l)}{2\alpha^3} \pm \frac{\beta\sqrt{\tanh(\varepsilon\alpha l)}}{2\alpha^{\frac{3}{2}}}\sqrt{\frac{\beta^2\tanh(\varepsilon\alpha l)}{\alpha^3} - 12}. \tag{4.8}$$

Since the existence of a solution for κ_2 requires $\frac{\beta^2\tanh(\varepsilon\alpha l)}{\alpha^3} > 12$, it is easy to see that $A(\kappa_2) > 6$, so by Theorem 1 the solution corresponding to κ_2 is unstable. For the other branch, corresponding to κ_1, we take $\frac{\beta^2\tanh(\varepsilon\alpha l)}{\alpha^3} = 12 + \delta$, where $\delta > 0$, then we have

$$A(\kappa_1) = 6 - \frac{\sqrt{12\delta + \delta^2} - \delta}{2} < 6.$$

Therefore, the solution corresponding to κ_1 is stable. Moreover, at the fold point where $\frac{\beta^2\tanh(\varepsilon\alpha l)}{\alpha^3} = 12$, we can easily get from (4.8) that $A = 6$, which corresponds to $\lambda = 0$. We summarise our result as follows.

Proposition 1 *In the case* $\tau = 0$, *the one-spike solution* $u(x), v(x)$ *given in (3.7), (3.11) with* $v(0) = \kappa_2$ *is unstable and the other branch* $v(0) = \kappa_1$ *is always stable. The two roots connect at a fold point corresponding to a double root of (3.15).*

4.3 The case $\tau \neq 0$

We now study the case with A depend on λ. To study the stability of the lower branch with $v(0) = k_2$, we first rewrite equation (4.5) in the following form:

$$(L_0 - \lambda)\phi = w^2, \qquad \text{where} \quad \int \phi w\, dy = A(\lambda)\,,$$

or

$$\int w(L_0 - \lambda)^{-1} w^2\, dy = A(\lambda). \tag{4.9}$$

(Here, we use the fact that ϕ is only defined up to a multiplicative constant and we scale ϕ so that $\int \phi w = A$).

We denote the left-hand side of equation (4.9) as $f(\lambda)$. The global behaviour of precisely this same $f(\lambda)$ was studied in [31], from which we obtain the following basic results:

Theorem 2 *(See [31]) $f(\lambda)$ has the behavior*

$$f(0) = 6, f'(\lambda) > 0, f''(\lambda) > 0, \lambda \in \left(0, \frac{5}{4}\right).$$

Moreover, $f(\lambda)$ has a singularity at $\lambda = \frac{5}{4}$ with $f(\lambda) \to \pm\infty$ as $\lambda \to \frac{5}{4}_{\pm}$. For $\lambda > \frac{5}{4}$, we have $f(\lambda) < 0$ and $f(\lambda) \to 0$ as $\lambda \to \infty$.

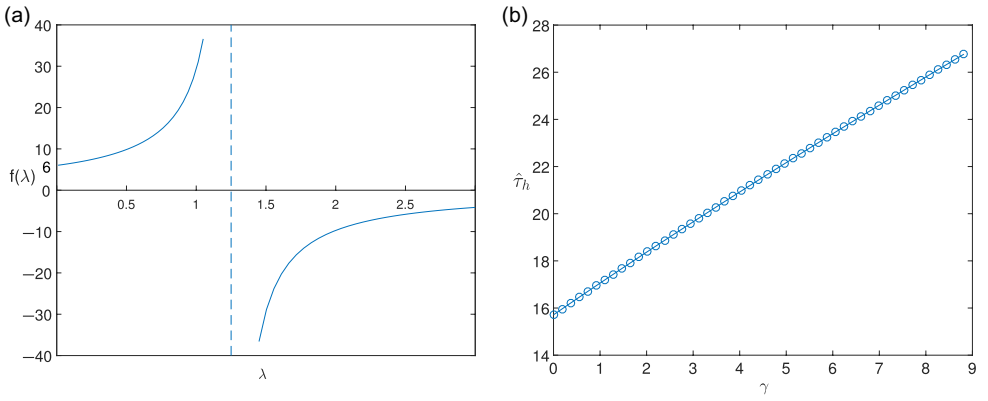

FIGURE 5. Computational results illustrating the stability analysis; see text for details. (a) The function $f(\lambda)$ given in left-hand side of (4.9). (b) Hopf bifurcation points $\hat{\tau}_h$ against γ.

The graph of $f(\lambda)$ is shown in Figure 5(a). Since from the right-hand side of equation (4.9), we have that $A(\lambda)$ is continuous and from the previous subsection we have that $A(0) > 6$. Therefore the two functions $f(\lambda)$ and $A(\lambda)$ must intersect in the domain $\lambda > 0$, so that equation (4.9) must have a positive eigenvalue, which shows that the lower branch with $v(0) = \kappa_2$ is unstable.

We now study the stability of the upper branch, with $v(0) = \kappa_1$. Since we are interested in large domain $l \to \infty$, we let $\tanh(\varepsilon\alpha l) \sim 1$, then we rewrite A as following by introducing $\hat{\tau} = \frac{\tau k^4}{\varepsilon^2}$, and $\gamma = \alpha^2 k^4$, to obtain

$$A \sim 3 + \sqrt{\hat{\tau}\lambda + \gamma}.$$

When $\hat{\tau}$ is sufficiently large, the system can be destabilised via a Hopf bifurcation. This was first proved in [31], from which we have the following result:

Theorem 3 *(See* [31]*) In the case $\hat{\tau} > 0$, the one-spike solution $u(x), v(x)$ given in (3.7), (3.11) with $v(0) = \kappa_2$ is always unstable and $v(0) = \kappa_1$ is stable only when $0 < \hat{\tau} < \hat{\tau}_h$ for some $\hat{\tau}_h > 0$. As $\hat{\tau}$ increases past $\hat{\tau}_h$, a Hopf bifurcation in the amplitudes of the spikes is triggered.*

Although we know of no explicit formula for the threshold $\hat{\tau}_h$ at which the Hopf bifurcation occurs, we can compute $\hat{\tau}_h$ numerically. We discretised the NLEP (4.5) using a finite differences method. This results in a matrix eigenvalue problem $M\vec{\phi} = \lambda\vec{\phi}$. Here, $\vec{\phi}$ is an n by 1 column vector corresponding to the discretisation of the eigenfunction $\phi(x)$, where n is the number of mesh points, and M is an n by n matrix corresponding to the discretisation of the linear operator in (4.5). When $\hat{\tau} = 0$, this is a straigtforward matrix eigenvalue problem whose eigenvalues we computed using MATLAB's `eig` command. However when $\hat{\tau} \neq 0$, the coefficients in M also depend on λ: $M = M(\lambda)$. In this case, we used an iterative approach: starting with some λ_0, we solve $M(\lambda_0)\phi = \lambda_1\phi$ for λ_1; then $M(\lambda_1)\phi = \lambda_2\phi$ for λ_2, etc., with $\lambda_i \to \lambda$ as $i \to \infty$.

For a fixed γ, we used the above method to compute $\hat{\tau}_h$ such that $Re(\lambda) = 0$. The result is shown in Figure 5(b), which shows the Hopf bifurcation point $\hat{\tau}_h$ for $\gamma \in (0, 9)$.

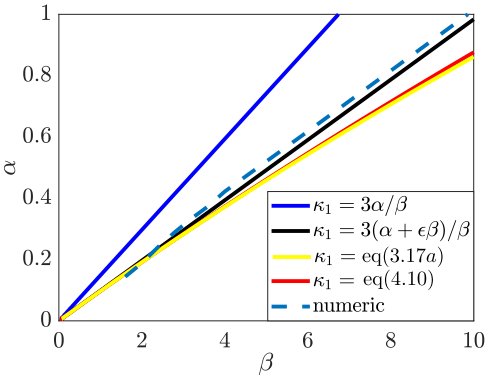

FIGURE 6. Hopf bifurcation threshold (Result 3). The parameters are $\varepsilon = 0.05, l = 100$. Here, dashed line are obtained through full simulations of system (2.1) by FlexPDE; different coloured solid line is obtained by computing α_h such that k solved in (4.11) satisfy (4.10), i.e. $v_0(\alpha_h) = 1.99\varepsilon^{\frac{1}{2}}$.

4.4 The case $\tau = 1$; comparison with numerics

In this paper, we consider system (2.1) with $\tau = 1$, which yields

$$\hat{\tau} = \frac{\kappa^4}{\varepsilon^2}. \tag{4.10}$$

In particular, we consider the regime $\beta \gg 1$ (independent of ε) and $\alpha \sim O(1)$, then to leading order we have from (3.17a) that

$$\kappa_1 \sim \frac{3\,(\alpha + \varepsilon\beta)}{\beta} + \frac{9\,(\alpha + \varepsilon\beta)^4}{\beta^3} + O\left(\frac{1}{\beta^5}\right) \approx \frac{3\alpha}{\beta}. \tag{4.11}$$

Therefore $\kappa_1^4 \ll 1$ and $\gamma = \alpha^2\kappa_1^4 \sim 0$, in which case $\hat{\tau}_h \sim 15.7$. From (4.10), we obtain the critical bifurcation value for alpha

$$\alpha_h \sim \frac{\varepsilon^{\frac{1}{2}}\hat{\tau}_h^{\frac{1}{4}}\beta}{3} = \frac{15.7^{\frac{1}{4}}\varepsilon^{\frac{1}{2}}\beta}{3} \sim 0.6636\varepsilon^{\frac{1}{2}}\beta.$$

We summarise our results as follows.

Proposition 2 *In the case $\tau = 1$, the one-spike solution $u(x), v(x)$ given in (3.7), (3.11) with $v(0) = \kappa_1$ is stable only when $0 < \alpha < \alpha_h$. As α increases past α_h, a Hopf bifurcation in the amplitude of the spikes is triggered. In particular, in the regime of large β, we have*

$$\alpha_h \sim 0.6636\varepsilon^{\frac{1}{2}}\beta.$$

To verify the proposition, we can compare with numerical computation of the spectrum using a finite-difference approach. The result is shown in Figure 6, which shows good agreement when we take various different approximations to κ_1 that are accurate to $O(\varepsilon)$

Note the apparent contrast between this asymptotic result and the depicted numerical stability result of the spike solutions in Figure 1(c) for which no Hopf bifurcation on the upper branch was found. To resolve the apparent descrepancy, note however that the numerical results in that

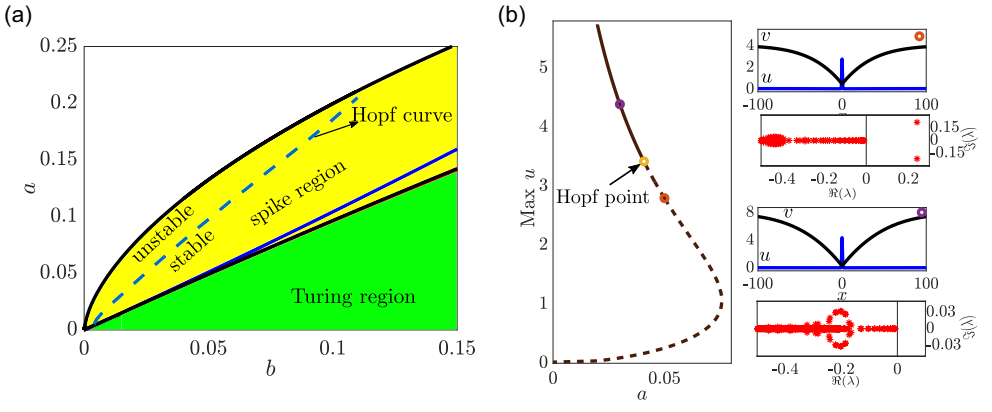

FIGURE 7. Color version online. A zoom of the numerical two-parameter bifurcation diagram for small a and b with region $\varepsilon = 0.05$ in the limit of $l = 100$. (a) The dashed (blue) curve indicates the location of the Hopf bifurcation. (b) Bifurcation diagram of max u vs. a for fixed $b = 0.01$ and $\varepsilon = 0.05$ showing the stable and unstable branches joining at the Hopf point $a_h = 0.0408$. The insets show represent solutions and corresponding linear spectrum either side of the Hopf bifucation.

figure were for $a = 0.3785$, which for $\varepsilon = 0.01$ is outside of the asymptotic regime of the present. Figure 7(a) shows a similar computation for $a \sim 0.1$ and $\varepsilon = 0.05$ which is consistent with the asymptotic limit. Here we see that as for small a there is indeed a Hopf bifurcation on the upper branch, before it connects to the lower branch in the fold. As a increases, the Hopf point gets closer to the fold and dissapears in a codimension-two point for $a \approx 0.2$. For larger a-values the upper branch is stable all the way up to the fold point. Here, the location of the Hopf instability was found by computing the spectrum of the spike solution and using a simple bisection method to find where a pair of imaginary eigenvalues cross the imaginary axis (see Figure 7(b). The numerical results also confirms that the Hopf eigenvector (not shown) is localised and represents oscillation of the core of the spike.

4.5 Numerical simulation results

To establish whether the Hopf bifurcation is super or sub-critical, we use the direct numerical simulation of (2.1). Based on the computation in Figure 7(b), it is possible to select two points; one just before the Hopf bifurcation and the other just after. Figure 8(a), (b) illustrates the results of the direct simulation of (2.1) as the maximum of the u component as a function of time for $b = 0.09$ and $\varepsilon = 0.05$, given small spatially uniform perturbations to the spike solutions u_0 and v_0. That is the initial condition is $(u(x, 0), v(x, u)) = u_0(x) + \delta, v_0(x) + \delta)$. For these values of the parameters, the Hopf occurs at $a_h = 0.1658$. Figure 8(a) shows that the spike solution before the Hopf point $a = 0.1657$, seems to be stable under small perturbations ($\delta \leq 0.085$), yet for a perturbation that is slightly bigger, the solution leaves the basin of attraction of the spike solution and completely collapses to the homogeneous steady state. As we move beyond the Hopf point, any size of perturbation is found to oscillate with increasing amplitude until it collapses completely back to the homogeneous steady state; see Figure 8(b). Hence, it can be concluded from the numerical simulation that the Hopf bifurcation is subcritical.

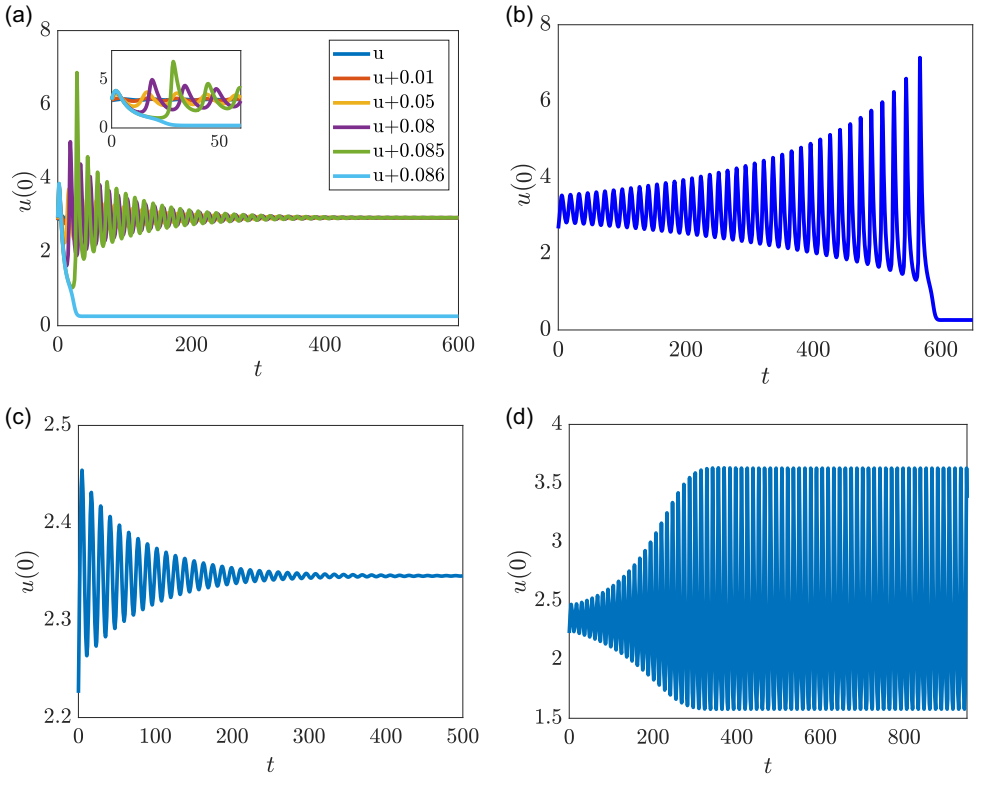

FIGURE 8. Direct simulation results for $\varepsilon = 0.05$ as a graph of the u value of the centre of the spike over time, given initial conditions that are a small perturbation from the steady pulse solution. (a) Solution to (2.1) with $a = 1.657$, $b = 0.09$ and $l = 120$; (b) the same except $a = 0.171$. (c) Solution to (4.1) with $a = 0.06$, $b = 0.02$, $l = 130$ and $\tau = 0.255$; (d) the same with $\tau = 0.28$.

Extensive simulations have revealed that the Hopf bifurcation is subcritical for all values of a and b forming the curve of Hopf bifurcations in Figure 7(a). However, we have found evidence that the Hopf bifurcation may become supercritical for larger values of ε. Alternatively if we take a value of a and b well inside the stable spike region of Figure 7(a), we find that reducing the value of τ can produce a Hopf bifurcation that is supercritical. See Figure 8(c), (d).

We have also performed further simulations of what can happen on a finite domain. Just like many other reaction diffusion models such as the desertification model [34] or the 'classical' Schankenberg model [30, 12], the extended Schankenberg model exhibits spike self-replication when b is increased. In addition, we have found a new mechanism leading to birth of new spikes – as illustrated in Figure 9 – that occurs for higher values of a: we call this 'spike insertion' whereby additional spikes appear from the 'background', away from other spikes. Contrast this with spike replication, where a spike splits into two. Numerical simulations suggest that spike insertion is more prevalent for smaller values of a and when there are fewer spikes already present, and in general spike replication can follow spike insertion as b is increased further. Unlike spike replication, spike insertion is specific to the extended Schnakenberg model and, as far as we are aware, does not occur in the classical Schnakenberg model (with $a = 0$) nor the Gray–Scott model.

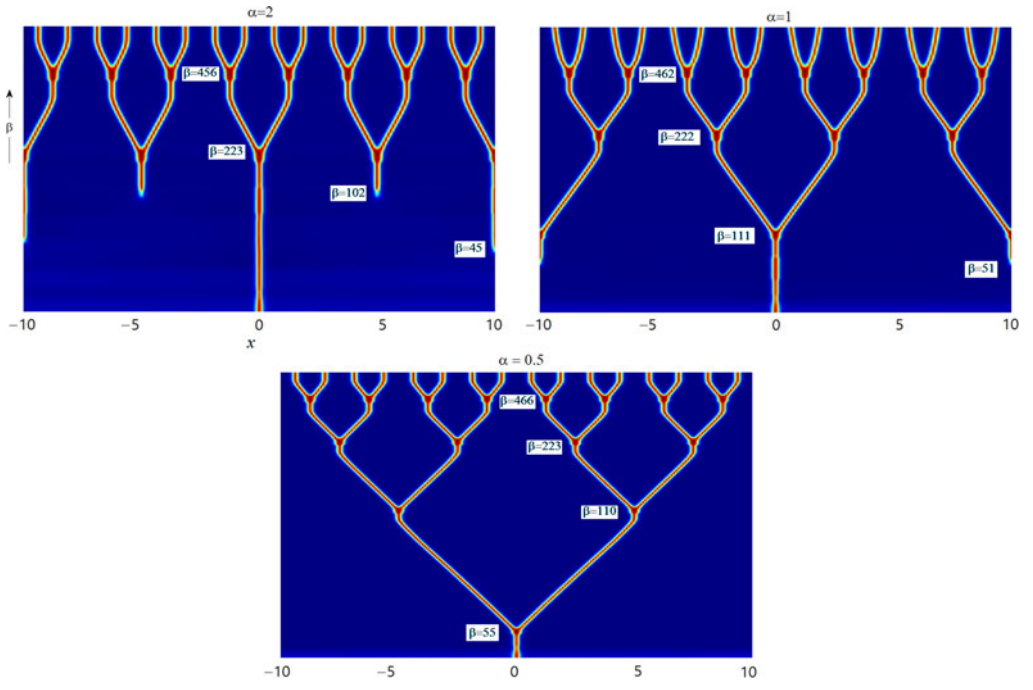

FIGURE 9. Spike insertion vs. spike splitting. Full numerical simulations of (2.1) with $\varepsilon = 0.05$, $l = 10$ and with b gradually increased according to the formula $\beta = 20 + 0.001 * t$, for several values of α as indicated in the sub-panels, where $a = \varepsilon\alpha$, $b = \varepsilon^2\beta$. $\alpha = 2$: two insertion events followed by self-replication events. $\alpha = 1$: one insertion event. $\alpha = 0.5$: no insertion events. Generally, for larger values of α several spike-insertion events can occur when β is relatively small, followed by self-replication events as β is further increased. For smaller values of α, only self-replication occurs as β is increased.

5 Conclusion

One of the aims of this work has been to show a connection between the semi-strong asymptotic analysis and the theory of homoclinic snaking in systems of reaction diffusion equations (see also [23, 26] for earlier results in this direction). The former can be used to find analytic expressions for the structure and stability of spike solutions in a rather specific asymptotic limit. The latter, applies in the large, but apart from in a neighbourhood of a degenerate Turing bifurcation cannot provide asymptotic estimates. The nature of the localised structures found by the two different theories are radically different too. The former finds isolated spike solutions where one field is much more localised. The latter finds solutions a plethora of localised solutions that many peaks. The results in this paper go some way to demonstrating how the very different structures captured by the different theories can connected in an appropriate multi-parameter bifurcation diagram.

The key to the results presented here, compared with many other papers to use the semi-strong asymptotic theory, has been to pose the problem on the infinite domain. Then we can find a fold as an appropriate parameter is varied. We find numerically that this fold forms the outer extent of the localised pattern region, which extends far away from the asymptotic limit and into the snaking region. Moreover, we have shown how the exponentially localised solutions found by taking an infinite domain, naturally transition to the solutions that are delocalised in the v field.

An additional feature we found is the presence of a Hopf bifurcation in the limit that the source parameters a and b are sufficiently small. The presence of this instability was argued using an extension to a previously analysed non-local eigenvalue problem. For the particular model studied though, this instability was found numerically to not penetrate into parameter regions with large a and b. Preliminary calculations suggest that further asymptotic explanation of this disappearance of the Hopf bifurcation might be possible, by taking a slightly different distinguished limit.

It is helpful for us describe the difference between the 'extended' Schankenberg model (2.1) and what we shall call the 'classical' Schankenberg model, which has no source term for the activator, i.e. $a = 0$ in (2.1), see, e.g. [30]. There are several key differences here. In particular, the introduction of the non-zero activator feed rate allows for a spike solution which exists on an unbounded domain $x \in \mathbb{R}$. For the classical Schankenberg model that is not the case; a single spike cannot be constructed on an unbounded domain. Note however that a single spike on the entire domain is possible for Gray–Scott model which also has a decay term in v. Moreover the outer region for u no longer decays to zero, and instead leads to a nonlinear outer problem and gives the possibility of a fold.

We have also found novel dynamics of the spike solutions. We have provided strong numerical evidence that the Hopf bifurcation may be either supercritical or subcritical Hopf bifurcations, depending on the paramaeter values. We have also found evidence of novel spike insertion dynamics. These dynamical features warrant further analytical investigation; which should form the subject of future work.

Finally, although the results presented here are relevant for a particular Schnakenberg model, we believe the results are likely to be ubiquitous for a large class of physically important reaction-diffusion equations. That ubiquity will be explored in forthcoming work [1].

Acknowledgements

The authors should like to thank Jens Rademacher (University of Breman), Michael Ward (University of British Columbia) and Nicolas Verschueren (University of California, Berkeley) for helpful discussions. We also thank both anonymous referees for making helpful suggestions.

Conflict of interest

None.

References

[1] Al Saadi, F., Champneys, A. & Verschueren, N. (2020) Localised patterns and semi-strong interaction, a unifying framework for reaction-diffusion systems. Preprint. University of Bristol.

[2] Beck, M., Knobloch, J., Lloyd, D., Sandstede, B. & Wagenknecht, T. (2009) Snakes, ladders, and isolas of localized patterns. *SIAM J. Math. Anal.* **41**, 936–972.

[3] Benson, D., Sherratt, J. & Maini, P. (1993) Diffusion driven instability in inhomogeneous domain. *Bull. Math. Biol.* **55**(2), 365–384.

[4] Breña–Medina, V. & Champneys, A. (2014) Subcritical Turing bifurcation and the morphogenesis of localized patterns. *Phys. Rev. E* **90**, 032923.

[5] Burke, J. & Knobloch, E. (2006) Snakes and ladders: localized states in the Swift–Hohenberg equation. *Physics Lett. A* **360**, 681–688.

[6] DOEDEL, E., OLDEMAN, B. ET AL. (2020) Auto-07p: continuation and bifurcation software for ordinary differential equations. https://github.com/auto-07p.
[7] DOELMAN, A., KAPER, T. J. & ZEGELING, P. A. (1997) Pattern formation in the one-dimensional gray-scott model. *Nonlinearity* **10**(2), 523.
[8] DOELMAN, A. & VEERMAN, F. (2015) An explicit theory for pulses in two component, singularly perturbed, reaction–diffusion equations. *J. Dyn. Differ. Equ.* **27**(3), 555–595.
[9] GIERER, A. & MEINHARDT, H. (1972) A theory of biological pattern formation. *Kybernetik* **12**(1), 30–39.
[10] HARAGUS, M. & IOOSS, G. (2011) *Local Bifurcations, Center Manifolds, and Normal Forms in Infinite-Dimensional Dynamical Systems*, Springer, New York.
[11] IRON, D., WARD, M. & WEI, J. (2001) The stability of spike solutions to the one-dimensional gierer-meinhardt model. *Physica D Nonlinear Phenomena* **150**(1), 25–62.
[12] IRON, D., WEI, J. & WINTER, M. (2004) Stability analysis of turing patterns generated by the schnakenberg model. *J. Math. Biol.* **49**(4), 358–390.
[13] KNOBLOCH, E. (2015) Spatial localization in dissipative systems. *Ann. Rev. Condens. Matter Phys.* **6**, 325–359.
[14] KNOBLOCH, E. (2016) Localized structures and front propagation in systems with a conservation law. *IMA J. Appl. Math.* **81**, 457–487.
[15] KOLOKOLNIKOV, T., SUN, W. & WARD, M. (2006) The stability of a stripe for the Gierer-Meinhardt model and the effect of saturation. *SIAM J. Appl. Dyn. Sys.* **5**, 313–363.
[16] KOLOKOLNIKOV, T., WARD, M. J. & WEI, J. (2005) The existence and stability of spike equilibria in the one-dimensional gray–scott model: the low feed-rate regime. *Stud. Appl. Math.* **115**(1), 21–71.
[17] KOLOKOLNIKOV, T. & WEI, J. (2018) Pattern formation in a reaction-diffusion system with space-dependent feed rate. *SIAM Rev.* **60**(3), 626–645.
[18] MERON, E. (2015) *Nonlinear Physics of Ecosystems*, 3rd ed., CRC Press, USA.
[19] MURATOV, C. & OSIPOV, V. V. (2000) Static spike autosolitons in the gray-scott model. *J. Phys. A Math. General* **33**(48), 8893.
[20] MURATOV, C. B. & OSIPOV, V. (2002) Stability of the static spike autosolitons in the gray–scott model. *SIAM J. Appl. Math.* **62**(5), 1463–1487.
[21] MURRAY, J. (2002) *Mathematical Biology II: Spatial Models and Biomedical Applications*, 3rd ed., Springer-Verlag, New York.
[22] POMEAU, Y. (1986) Front motion, metastability and subcritical bifurcations in hydrodynamics. *Physica D Nonlinear Phenomena* **23**, 3–11.
[23] RADEMACHER, J. (2013) First and second order semistrong interaction in reaction-diffusion systems. *SIAM J. Appl. Dyn. Syst.* **12**, 175–203.
[24] SCHNAKENBERG, J. (1979) Simple chemical reaction system with limit cycle behavior. *Theor. Biol.* **81**(12), 389–400.
[25] SHAW, L. & MURRY, J. (1990) Analysis of a model for complex skin pattern. *SIAM J. Appl. Math.* **50**(2), 628–648.
[26] SITEUR, K., SIERO, E., EPPINGA, M., RADEMACHER, J., DOELMAN, A. & RIETKERK, M. (2014) Beyond Turing: the response of patterned ecosystems to environmental change. *Ecol. Complexity* **20**, 81–96.
[27] SWIFT, J. & HOHENBERG, P. C. (1977) Hydrodynamic fluctuations at the convective instability. *Phys. Rev. A* **15**, 319–328.
[28] TURING, A. M. (1952) The chemical basis of morphogenesis. *Philos. Trans. R. Soc. London B Biol. Sci.* **237**, 37–72.
[29] VERSCHUEREN, N. & CHAMPNEYS, A. (2020) Dissecting the snake: from localized to patterns in isolated spikes in pattern formation systems. https://arxiv.org/abs/1809.07847.
[30] WARD, M. & WEI, J. (2002) The existence and stability of asymmetric spike patterns for the Schnakenberg model. *Stud. Appl. Math.* **109**, 229–264.
[31] WARD, M. & WEI, J. (2003) Hopf bifurcations and oscillatory instabilities of spike solutions for the one-dimensional gierer-meinhardt model. *J. Nonlinear Sci.* **13**(2), 209–264.

[32] WEI, J. (1999) On single interior spike solutions of the gierer–meinhardt system: uniqueness and spectrum estimates. *Eur. J. Appl. Math.* **10**(4), 353–378.
[33] WOODS, P. & CHAMPNEYS, A. (1999) Heteroclinic tangles and homoclinic snaking in the unfolding of a degenerate reversible Hamiltonian–Hopf bifurcation. *Physica D Nonlinear Phenomena* **129**, 147–170.
[34] ZELNIK, Y. R., UECKER, H., FEUDEL, U. & MERON, E. (2017) Desertification by front propagation? *J. Theor. Biol.* **418**, 27–35.